© 2021. Published by The Company of Biologists Ltd | Journal of Experimental Biology (2021) 224, jeb242968. doi:10.1242/jeb.242968

RESEARCH ARTICLE

MicroRNA-mediated inhibition of AMPK coordinates tissue-specific downregulation of skeletal muscle metabolism in hypoxic naked mole-rats

Hanane Hadj-Moussa[1], Sarah Chiasson[2], Hang Cheng[2,‡], Liam Eaton[2,‡], Kenneth B. Storey[1,*,§] and Matthew E. Pamenter[2,3,*,§]

ABSTRACT

Naked mole-rats reduce their metabolic requirements to tolerate severe hypoxia. However, the regulatory mechanisms that underpin this metabolic suppression have yet to be elucidated. 5′-AMP-activated protein kinase (AMPK) is the cellular 'master' energy effector and we hypothesized that alterations in the AMPK pathway contribute to metabolic reorganization in hypoxic naked mole-rat skeletal muscle. To test this hypothesis, we exposed naked mole-rats to 4 h of normoxia (21% O_2) or severe hypoxia (3% O_2), while indirectly measuring whole-animal metabolic rate and fuel preference. We then isolated skeletal muscle and assessed protein expression and post-translational modification of AMPK, and downstream changes in key glucose and fatty acid metabolic proteins mediated by AMPK, including acetyl-CoA carboxylase (ACC1), glycogen synthase (GS) and glucose transporters (GLUTs) 1 and 4. We found that in hypoxic naked mole-rats (1) metabolic rate decreased ∼80% and fuel use switched to carbohydrates, and that (2) levels of activated phosphorylated AMPK and GS, and GLUT4 expression were downregulated in skeletal muscle, while ACC1 was unchanged. To explore the regulatory mechanism underlying this hypometabolic state, we used RT-qPCR to examine 55 AMPK-associated microRNAs (miRNAs), which are short non-coding RNA post-transcriptional silencers. We identified changes in 10 miRNAs (three upregulated and seven downregulated) implicated in AMPK downregulation. Our results suggest that miRNAs and post-translational mechanisms coordinately reduce AMPK activity and downregulate metabolism in naked mole-rat skeletal muscle during severe hypoxia. This novel mechanism may support tissue-specific prioritization of energy for more essential organs in hypoxia.

KEY WORDS: Hypoxic metabolic response, *Heterocephalus glaber*, miRNA, Hypometabolism, GLUT4, Glycolysis, Glycogen synthase

INTRODUCTION

Eusocial East-African naked mole-rats (*Heterocephalus glaber*) live in crowded underground tunnel systems, wherein they putatively experience intermittent hypoxic conditions in their nesting chambers. Whereas the absolute levels of hypoxia within their underground burrow systems are poorly studied (Holtze et al., 2018), laboratory studies have demonstrated that naked mole-rats are remarkably hypoxia tolerant (for an adult mammal), and can withstand minutes of anoxia, hours at 3% O_2, and days to weeks at 8–10% O_2 (Chung et al., 2016; Pamenter et al., 2015; Park et al., 2017). Naked mole-rats possess an impressive arsenal of adaptations that allow them to survive oxygen deprivation. Perhaps most critically, and similar to other champions of hypoxia and anoxia tolerance (Boutilier, 2001; Buck and Pamenter, 2006; Hochachka et al., 1996), naked mole-rats reduce their metabolic rate in oxygen-limiting environments (Pamenter et al., 2015), which presumably enables their energy demands to be met by less efficient anaerobic pathways (Pamenter et al., 2019). In support of this, naked mole-rat blood glucose levels are elevated during 4 h of progressively deeper hypoxia (9–3% O_2) (Pamenter et al., 2019), and anoxia (Park et al., 2017), tissue ATP concentrations are largely maintained, and respiratory exchange ratio (RER) calculations indirectly support a whole-animal metabolic fuel switch from primarily lipid-based metabolism in normoxia to carbohydrate-based metabolism in hypoxia (Pamenter et al., 2019). However, the cellular mechanisms that regulate this putative hypoxic metabolic fuel switch remain unknown.

Cells use various processes to regulate metabolism and balance the activation and suppression of energetically expensive biological processes when ATP availability is limited. One of the primary initiators of such metabolic remodelling is 5′-AMP-activated protein kinase (AMPK), which is a master cellular energy sensor. AMPK is activated by changes in the intracellular AMP:ATP ratio, such that breakdown of ATP to AMP favours activation of AMPK, which in turn modifies cellular energetics and metabolic fuel use (Hardie et al., 2012). For example, AMPK activation during low-energy stress, such as occurs during hypoxia or anoxia, leads to a decrease in ATP-consuming anabolic pathways (e.g. fatty acid synthesis, which is gated by acetyl-CoA carboxylase 1, ACC1; Hardie, 2007). Specifically, AMPK-mediated phosphorylation inhibits ACC1 activity, thereby inhibiting lipogenesis, and stimulates fatty acid oxidation to conserve and alter fuel use during metabolic rate supression and environmental stress (Winder et al., 2003). This is typically associated with a stimulation of glucose uptake via glucose transporter proteins (GLUTs) in muscle, along with the inhibition of glycogen synthase (GS) to favour glycolysis (Kahn et al., 2005; Rider, 2016).

A key mechanism implicated in modulating cellular processes during hypoxia is microRNAs (miRNAs), which are short non-coding RNA transcripts. miRNAs post-transcriptionally regulate gene expression temporarily through suppression of mRNA translation via transcript storage, or through permanent degradation,

[1]Department of Biology and Institute of Biochemistry, Carleton University, Ottawa, ON, Canada, K1S 5B6. [2]Biology Department, University of Ottawa, Ottawa, ON, Canada, K1N 9A7. [3]Brain and Mind Research Institute, University of Ottawa, Ottawa, ON, Canada, K1H 8M5.
‡,*These authors contributed equally to this work

§Authors for correspondence (mpamenter@uottawa.ca; kennethstorey@cunet.carleton.ca)

M.E.P., 0000-0003-4035-9555

Received 2 June 2021; Accepted 7 July 2021

Journal of Experimental Biology (2021) 224, jeb242968. doi:10.1242/jeb.242968

depending on the degree of miRNA complementary binding (O'Brien et al., 2018). miRNAs are of particular interest in natural models of metabolic reorganization because they: (1) are reversible, (2) are rapidly acting, (3) are energetical inexpensive to synthesize, and (4) can target virtually all biological pathways (Hadj-Moussa and Storey, 2020). Studies on other hypoxia- and anoxia-tolerant organisms have identified subsets of species- and tissue-specific oxygen-responsive miRNAs known as 'OxymiRs', which are involved in protective roles and energy reprioritization when physiological oxygen levels decline; however, it is also clear that there is not a unified miRNA response to oxygen limitation (Hadj-Moussa and Storey, 2020).

In the present study, we examined a potential role for AMPK in mediating metabolic rate suppression and the hypoxic fuel switch previously identified in freely behaving naked mole-rats and explored a potential regulatory role for miRNAs that target AMPK pathways. We hypothesized that naked mole-rat skeletal muscle would exhibit an AMPK-mediated fuel substrate switch to favour carbohydrate metabolism and enhance glycolysis, and predicted that this switch would be mediated by miRNA regulation of AMPK.

MATERIALS AND METHODOLOGY

Animals

Naked mole-rats, *Heterocephalus glaber* Rüppell 1842, were group-housed in interconnected multi-cage systems at 30°C and 21% O_2 in 50% humidity with a 12 h dim light:12 h dark cycle. Animals were fed fresh tubers, vegetables, fruit and Pronutro cereal supplement *ad libitum*. Animals were not fasted prior to experimental trials. All experimental procedures were approved by the University of Ottawa Animal Care Committee in accordance with the Animals for Research Act and by the Canadian Council on Animal Care. All experiments were performed during daylight working hours in the middle of the animals' 12 h:12 h light:dark cycle. We examined miRNA and protein changes following *in vivo* hypoxic exposure in non-breeding naked mole-rats that were 1–2 years old. Non-breeding (subordinate) naked mole-rats do not undergo sexual development or express sexual hormones and thus we did not take sex into consideration when evaluating our results (Holmes et al., 2009).

Whole-animal respirometry

Naked mole-rats (n=6) were individually placed, unrestrained, into a 450 ml Plexiglas respirometer chamber, which was situated within a larger environmental chamber held at 30°C (range 29.8–30.2°C). The chamber temperature was recorded every 2 s using a custom-designed thermocouple. Animals were provided with a thin layer of corn cob bedding and the respirometer was continuously ventilated with gas mixtures set to the desired fractional gas composition by calibrated rotameters (Krohne, Duisburg, Germany). Inflowing gas was set at a flow rate of 100 ml min^{-1}, determined using a calibrated mass flow meter (Alicat Scientific, Tuscon, AZ, USA), and consistent with previous measurements in this species (Chung et al., 2016; Dzal et al., 2019). The excurrent gas was passed through a desiccant (Drierite, W.A. Hammond Drierite Co. Ltd, Xenia, OH, USA) before entering the cells of the O_2 and CO_2 analysers (FC-10 Oxygen Analyzer and CA-10 Carbon Dioxide Analyzer, Sable Systems), which were used to determine the gas concentrations of inspired and expired air. Before each trial, the O_2 and CO_2 analysers were calibrated using 100% N_2, compressed air (20.95% O_2) and a span gas (1.5% CO_2; balance N_2).

Prior to experimentation, animals were placed in the respirometry chamber for 1 h to familiarize them with their new surroundings. Oxygen consumption ($\dot{V}_{O_2}$) and carbon dioxide production ($\dot{V}_{CO_2}$) rates were then recorded for the next hour (normoxic control period). The incurrent gas was then switched to 3% O_2 (0.05% CO_2, balance N_2) and flow rate was increased to 1 l min^{-1} for 10 min to rapidly reduce the O_2 content of the chamber to 3% O_2. The flow rate was then returned to 0.1 l min^{-1} for the remaining 4 h of hypoxic exposure. ($\dot{V}_{O_2}$ and $\dot{V}_{CO_2}$ were measured during the last 30 min (in three 10 min intervals) of each hour and these values were averaged for each animal. For 5 min at the end of each hour, incurrent gas concentrations were measured by bypassing the experimental chamber and diverting air flow directly to the O_2 and CO_2 analysers. $\dot{V}_{O_2}$ and $\dot{V}_{CO_2}$ were calculated using eqns 10.6 and 10.7 in Lighton (2008), respectively:

$$\dot{V}_{O_2} = \dot{V}_I[(F_{I_{O_2}} - F_{E_{O_2}}) - F_{E_{O_2}}(F_{E_{CO_2}} - F_{I_{CO_2}})]/(1 - F_{E_{O_2}}), \quad (1)$$

$$\dot{V}_{CO_2} = \dot{V}_I[(F_{E_{CO_2}} - F_{I_{CO_2}}) - F_{E_{CO_2}}(F_{I_{O_2}} - F_{E_{O_2}})]/(1 - F_{E_{CO_2}}), \quad (2)$$

where $\dot{V}_{O_2}$ is O_2 consumption rate (ml min^{-1}) and $\dot{V}_{CO_2}$ is CO_2 production rate (ml min^{-1}), $\dot{V}_I$ is incurrent flow rate (ml min^{-1}), $F_{I_{O_2}}$ and $F_{I_{CO_2}}$ are fractional concentrations of incurrent O_2 and CO_2 of dry gas, respectively, and $F_{E_{O_2}}$ and $F_{E_{CO_2}}$ are fractional concentrations of excurrent O_2 and CO_2 of dry gas, respectively (Lighton, 2008). The RER was calculated by dividing $\dot{V}_{CO_2}$ by $\dot{V}_{O_2}$. All metabolic variables are reported at standard temperature, pressure, dry (STPD).

Experimental design for tissue collection

To analyse the effects of hypoxia on skeletal muscle metabolic function, naked mole-rats were exposed to one of two treatment conditions: (1) normoxia (4 h in 21% O_2, balance N_2; n=6), or (2) acute hypoxia (4 h in 3% O_2, balance N_2; n=6). Immediately following treatment, animals were killed by cervical dislocation followed by immediate decapitation. Temporalis muscles were rapidly dissected (within 30 s), and immediately flash frozen in liquid nitrogen and then stored at −80°C until analysis.

Total RNA isolation

Total RNA was isolated from normoxic and hypoxic naked mole-rat temporalis muscles (50 mg; n=4 each). RNA was isolated using Trizol-chloroform (15596-018, Invitrogen), as per the manufacturer's instructions and as described in Hadj-Moussa et al. (2020). Precipitated RNA pellets were then resuspended in 50 µl RNase-free water. RNA purity was determined by examining the $A_{260/280}$ ratio and concentration were assessed using a Take3 micro-volume plate and spectrophotometer (BioTek). RNA integrity was verified by running RNA samples on a 1% agarose gel with SYBR Green (S7563, Invitrogen) and examining the presence of sharp bands for 28S and 18S rRNA.

miRNA quantification and data analysis

miRNA sample preparation used 3 µg of total RNA. An Epi-Bio PolyA tailing kit (PAP5104H, Epicenter) was used for polyadenylation, as per the manufacturer's instructions. The polyadenylated RNA sample (10 µl) was combined with 5 µl of 250 pmol l^{-1} universal stem-loop adapter primer (Table S1). Stem-loop adapter ligation occurred on a thermocycler, heated to 95°C for 5 min, incubated for 5 min at 65°C, then chilled on ice. Reverse transcription was performed as per the manufacturer's instructions

using the M-MLV reverse transcriptase (28025013, Invitrogen) and the following PCR program: 16°C for 30 min, 42°C for 30 min, and 85°C for 5 min.

Forward miRNA-specific primers were designed using naked mole-rat transcriptomic data and the universal reverse primer was designed using the described method (Table S1; Biggar et al., 2014; Hadj-Moussa et al., 2021). miRNA quantitative PCR (qPCR) reactions were prepared as described by Hadj-Moussa and Storey (2020) and performed on a CFX Connect™ Real-Time PCR Detections System (1855201, Bio-Rad) following MIQE guidelines (Bustin et al., 2009). The miRNA PCR program was as follows: an initial 3 min at 95°C and then 60 cycles of 95°C for 10 s and 60°C for 30 s.

Differential miRNA expression levels (n=3–4) were calculated using the ΔΔCq comparative method. Cycle threshold (Cq) values were transformed to the 2^{-Cq} form, to allow for the normalization of the miRNA of interest to the endogenous controls (Peltier and Latham, 2008; Schmittgen and Livak, 2008). The mean of *Snord58a* and *Snord96a* expression was found to be the most stable endogenous control between normoxic and hypoxic conditions. Data were collected and analysed as mean (±s.e.m.) relative expression (n=3–4 independent biological replicates from different animals at each sampling point).

Soluble protein isolation

Protein extraction was performed as per the manufacturer's instructions (48-630MAG, EMD Millipore). Briefly, 75 mg of frozen tissue from normoxic and hypoxic naked mole-rats (n=6 each) was homogenized in 1:5 (w/v) 1× lysis buffer (43-045, EMD Millipore). Lysis buffer was pre-chilled and combined with 1 mmol l^{-1} Na_3VO_4, 10 mmol l^{-1} NaF, 10 mmol l^{-1} β-glycerophosphate and 10 µl ml^{-1} of protease inhibitor cocktail containing 104 mmol l^{-1} AEBSF, 80 µmol l^{-1} aprotinin, 4 mmol l^{-1} bestatin, 1.4 mmol l^{-1} E-64, 2 mmol l^{-1} leupeptin and 1.5 mmol l^{-1} pepstatin A (Bioshop PIC001.1). Homogenates were placed on ice for 30 min and vortexed every 10 min. Samples were then centrifuged at 14,000 ***g*** for 20 min at 4°C. Soluble protein containing supernatants was collected, aliquoted and stored at −80°C until later use.

Protein concentrations were measured using the Bio-Rad Protein Assay Kit II (5000002) as per the manufacturer's instructions. Protein concentrations were standardized using homogenization lysis buffer. Samples were then mixed 1:1 (v/v) with SDS buffer and 10% β-mercaptoethanol. Samples were then boiled for 10 min and stored at −20°C until use.

Western blotting and data analysis

Total protein homogenates (25 µg) of each sample were loaded onto 6–12% polyacrylamide gels and prepared with 5% upper staking gels. For additional information on the SDS-PAGE and immunoblotting protocol, refer to Hadj-Moussa and Storey (2018). The following primary antibodies were used AMPK-α1 (AF3197, R&D Systems), AMPK-α2 (AF2850, R&D Systems), AMPK-β (GTX134594, GeneTex), phospho-AMPK (Thr172; p-AMPK) (P01420-2, Boster), GLUT1 (A6982, AbClonal), GLUT4 (sc-7938, Santa Cruz Biotechnology Inc.), ACC (GTX132081, GeneTex), phospho-ACC (Ser79; p-ACC) (GTX133974, GeneTex), glycogen synthase (ab227270, AbCam) and phospho-glycogen synthase (Ser641/645; pGS) (07-817, Millipore-Sigma). After incubation overnight in the target primary antibody, membranes were washed with TBST and incubated with the appropriate HRP-linked anti-rabbit, anti-mouse or anti-goat secondary antibody (BioShop; 1:8000 v/v dilution in TBST) for 30 min at room temperature. Membranes were then washed in TBST and protein bands were visualized with enhanced chemiluminescence (H_2O_2 and Luminol) on a ChemiGenius Bio-Imaging System (Syngene). Membranes were then stained with Coomassie Brilliant Blue (0.25% w/v Coomassie Brilliant Blue, 7.5% v/v acetic acid, and 50% v/v methanol) to visualize total protein levels.

Relative protein abundance of chemiluminescent bands was quantified by densitometry using Gene Tools Software (Syngene). Minor variations in sample loading were corrected by standardizing the target protein band with the band intensity of a group of Coomassie Brilliant Blue-stained protein bands from each lane.

Statistical analysis

Respirometry data were analysed using a one-way repeated measures ANOVA with Tukey *post hoc* test. miRNA relative expression between normoxic and hypoxic conditions was considered significant when an unpaired Student's *t*-test resulted in P<0.05 using the RBioplot statistical and graphing R package (Zhang and Storey, 2016). Western blot data were analysed with an unpaired Student's *t*-test. Statistical analyses of whole-animal and immunoblot data were performed using commercial software (Prism v.8.4.2, GraphPad Software Inc., CA, USA). All values are presented as means±s.e.m., where P<0.05 was the threshold for significance.

RESULTS

Naked mole-rats exhibit robust metabolic rate suppression and a fuel switch from mixed lipids to carbohydrates in acute hypoxia

Relative to the normoxia baseline, naked mole-rats exhibited significant decreases of 63–80% in $\dot{V}_{O_2}$ and $\dot{V}_{CO_2}$ during 4 h of acute and severe hypoxia exposure (3% O_2 inhaled; Fig. 1A,B; $F_{1,5}$=60.7, P<0.0005 for $\dot{V}_{O_2}$, $F_{1,5}$=121.2, P<0.0001 for $\dot{V}_{CO_2}$; n=6 for each). In addition, the RER was 0.67 in normoxia (Fig. 1C), indicating that naked mole-rats predominately used lipid substrates as a metabolic fuel source. With the onset of severe hypoxia, naked mole-rats immediately exhibited a shift towards near-total reliance on carbohydrates (RER of ∼1.02 and 1.05 at 3 and 4 h of hypoxia, respectively; Fig. 1C; $F_{1,5}$=9.6, P<0.0045; n=6).

AMPK subunit expression and phosphorylation are altered during acute hypoxia

Relative expression levels of regulatory AMPK subunits and p-AMPK were examined using immunoblotting in normoxic and hypoxic naked mole-rat temporalis muscle. Protein levels of the AMPK-α1 and -β subunits remained constant during hypoxia (Fig. 2A; P=0.46 and 0.37, respectively; n=6 for each), while the AMPK-α2 subunit was downregulated by 59% (t_{10}=3.66, P=0.0044) and p-AMPK (Thr172) was downregulated by 58% (t_9=2.9, P=0.017; n=6 for each).

Carbohydrate but not lipid catabolic enzymes are reduced during hypoxia

The capacity for glucose uptake was examined by measuring the levels of GLUT1, which remained constant (Fig. 3; P=0.812; n=6), and GLUT4, which was downregulated by 45% in hypoxic naked mole-rat muscles (t_{10}=3.02, P=0.013; n=6). To examine whether hypoxic muscles were mobilizing glucose reserves for synthesis into glycogen, levels of GS and its activated phosphorylated form p-GS (Ser641/645) were also examined. While levels of GS remained constant (P=0.44; n=6), the activated phosphorylated form was significantly downregulated during hypoxia by 35%

Journal of Experimental Biology (2021) 224, jeb242968. doi:10.1242/jeb.242968

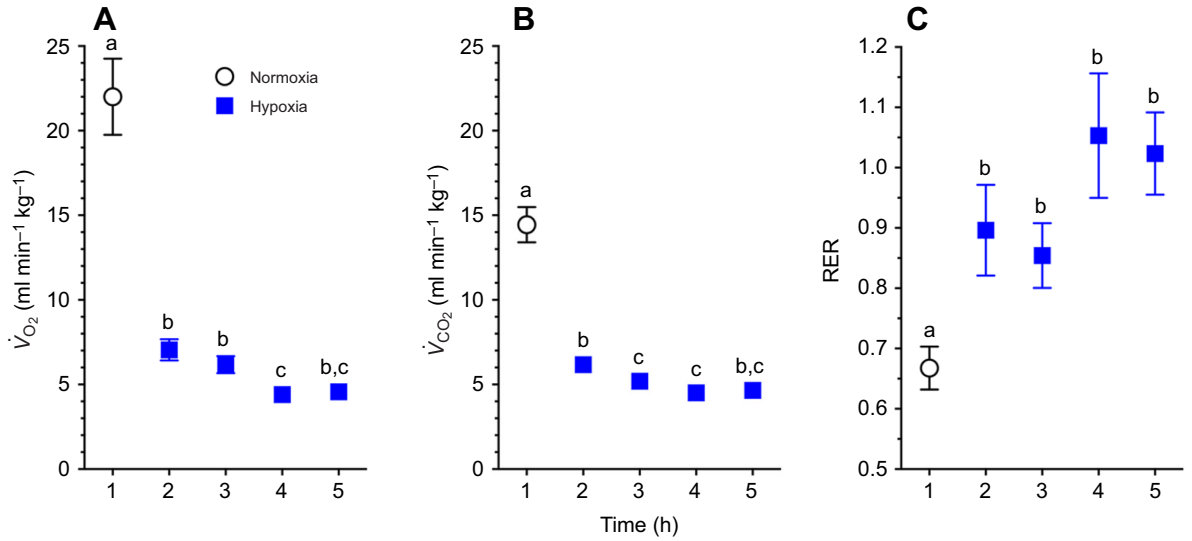

Fig. 1. Naked mole-rats exhibit metabolic rate suppression and a hypoxic fuel shift from lipids to carbohydrates in acute hypoxia. Summary of oxygen consumption rate ($\dot{V}_{O_2}$; A), carbon dioxide production rate ($\dot{V}_{CO_2}$; B) and respiratory exchange ratio (RER=$\dot{V}_{CO_2}/\dot{V}_O$; C) for 6 naked mole-rats exposed to 1 h of normoxia (21% O_2) and then 4 h of hypoxia (3% O_2). Data are presented as means±s.e.m. Significant differences are indicated by different letters (P<0.05, one-way ANOVA with Tukey's *post hoc* test).

(t_{10}=2.26, P=0.047; n=6). Finally, the effect of AMPK on lipogenesis was investigated by examining levels of ACC1 and its activated phosphorylated form p-ACC1 (Ser79), both of which were unchanged by hypoxic conditions (P=0.59 and 0.466, respectively; n=6 for each).

miRNAs are differentially expressed during hypoxia

A subset of AMPK-associated microRNAs (10 out of 55) were found to be differently regulated during hypoxia as compared with normoxic values using RT-qPCR (Fig. 4A). The three hypoxia-upregulated microRNAs were miR-124-3p. miR-101a-3p and miR-199a-5p (Fig. 4B). The seven hypoxia-downregulated microRNAs were: miR-137-3p, miR-200c-3p, miR-214-3p, miR-223-3p, miR-296-5p, miR-325-3p and miR-503-3p (Fig. 4B). For a complete list of miRNAs quantified (mean±s.e.m. relative expression and P-values), please refer to Table S2.

DISCUSSION

Severe hypoxia imposes significant restraints on aerobic energy production and most hypoxia-tolerant species employ strategies to reduce systemic metabolic demands when oxygen is limited (Boutilier, 2001; Buck and Pamenter, 2006; Hochachka et al., 1996). Naked mole-rats likely experience intermittent and severe hypoxia in their natural habitat and are capable of robust metabolic depression in hypoxia, but avoid torpor and maintain physical activity, albeit at a reduced degree (Houlahan et al., 2018; Ilacqua et al., 2017; Kirby et al., 2018). A long-standing theory in the field posits that hypoxia-tolerant organisms prioritize energy to support the function of essential organs in hypoxia, such as the brain and heart, while reducing the energy demand of less hypoxia-sensitive tissues, such as skeletal muscle. However, a mechanism underlying tissue-specific metabolic reorganization has not been described. Here, we used a multi-pronged approach to examine naked mole-rat energy reprioritization in skeletal muscle during severe hypoxia. We report three salient findings: first, metabolic rate decreases >80% during 4 h of severe hypoxia and whole-animal fuel consumption switches from lipid-based to carbohydrate-based metabolism, consistent with previous studies in hypoxic naked mole-rats (Chung et al., 2016; Dzal et al., 2019; Ilacqua et al., 2017; Kirby et al., 2018; Pamenter et al., 2015, 2019, 2018; Vandewint et al., 2019). Second, key regulatory components of AMPK, and of downstream AMPK-regulated mediators of carbohydrate metabolism are downregulated. Third, AMPK-regulating miRNAs are modified in a manner that is expected to reduce the overall activity of the AMPK pathway. Our findings imply a shift to an energy-conserving state, with reduced capacity for carbohydrate metabolism in naked mole-rat skeletal muscle during severe hypoxia, and offer a mechanism via which tissue-specific hypometabolism may be achieved.

Hypoxia downregulates AMPK and downstream regulators of carbohydrate metabolism

AMPK is a heterotrimer composed of a catalytic α-subunit and two regulatory β- and γ-subunits (Ross et al., 2016). Whereas expression of the α1- and β-subunits remains unchanged by hypoxia in naked mole-rat skeletal muscle, the α2-subunit is downregulated, along with p-AMPK, which is phosphorylated at Thr172, a key regulatory site on the α-subunit. Phosphorylation at Thr172 can trigger an ∼100-fold increase in AMPK activity and promote a cellular switch from ATP consumption to ATP production (Suter et al., 2006). AMPK directly modulates components of cellular carbohydrate and fatty acid metabolism and the decrease in p-AMPK reported here suggests that naked mole-rat muscles are not inducing energy-consuming biosynthetic fatty acid or glucose oxidation in hypoxia.

Activation of AMPK, and specifically its phosphorylation at Thr172, stimulates GLUT activity to enhance glucose uptake into cells (Abbud et al., 2000; Zhang et al., 1999). AMPK also modulates cellular glycolytic activity by phosphorylating GS at Ser7 (Ha et al., 2015), with phosphorylation of GS leading to a catalytically inactive enzyme. Similarly, AMPK can alter fatty acid usage through its interaction with ACC1, which gates the fatty acid synthesis pathway by catalysing the irreversible carboxylation of acetyl-CoA to produce malonyl-CoA, the building block for fatty acid chains (Hardie et al., 2012). Our findings that GLUT4 expression and GS phosphorylation both decreased in hypoxic skeletal muscle agree with our finding of decreased AMPK

Journal of Experimental Biology (2021) 224, jeb242968. doi:10.1242/jeb.242968

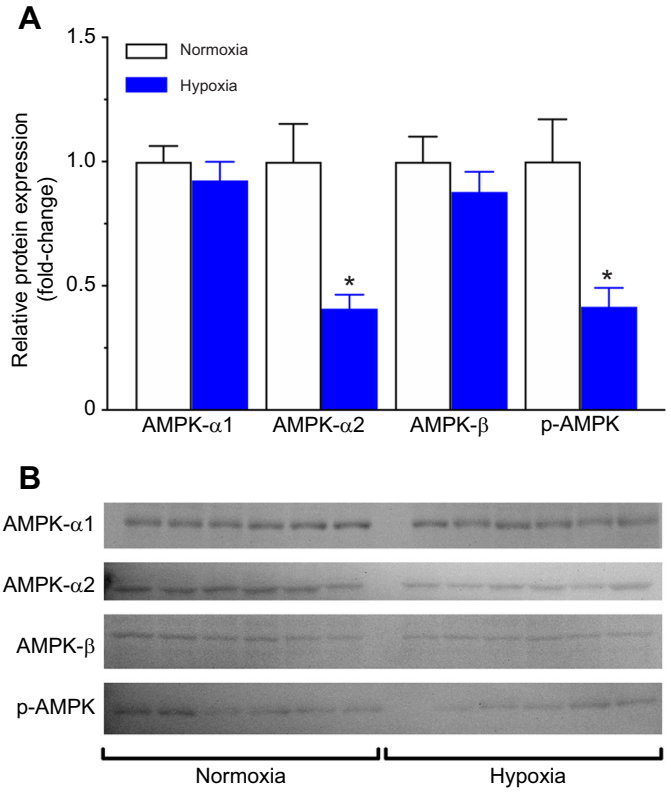

Fig. 2. 5′-AMP kinase (AMPK) function is downregulated in naked mole-rat skeletal muscle after acute hypoxia. (A) Relative expression (fold-change from normoxia) of AMPK subunit (α1, α2, β) and phosphorylated AMPK (Thr172, p-AMPK) protein expression in temporalis muscle of naked mole-rats exposed to 4 h hypoxia. (B) Immunoblots of protein expression from A. Data in A are means±s.e.m. from *n*=5–6 independent biological replicates for each condition. Significant differences from normoxic controls are indicated by asterisks (**P*<0.05, unpaired Student's *t*-test).

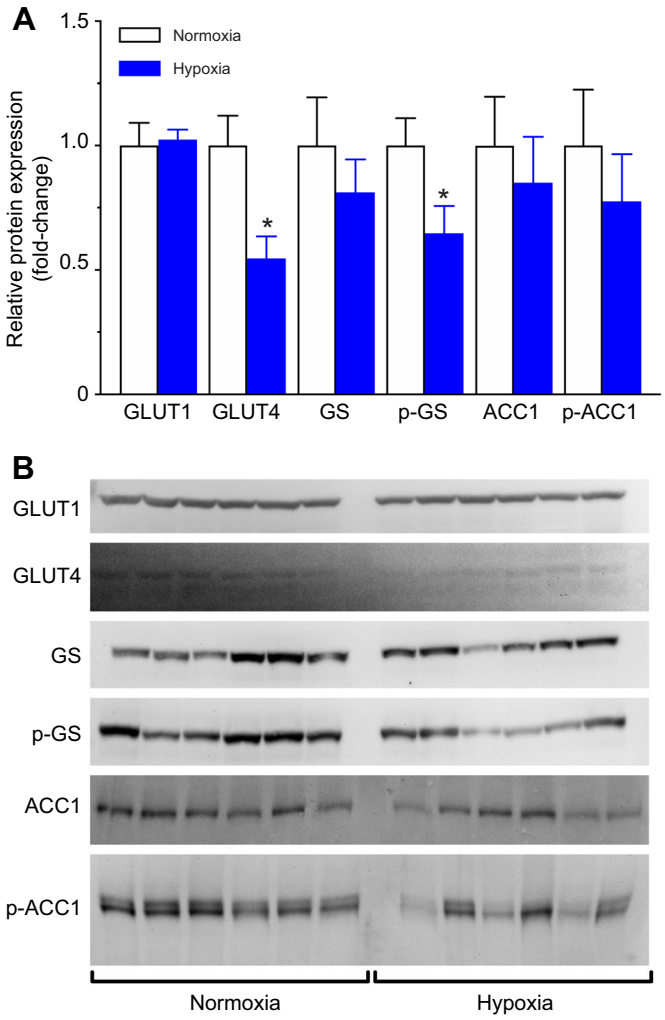

Fig. 3. Glucose metabolism is downregulated in naked mole-rat skeletal muscle after acute hypoxia. (A) Relative expression (fold-change from normoxia) of glucose transporters (GLUT1 and GLUT4), glycogen synthase (GS) and phosphorylated GS (Ser641/645, p-GS), and acetyl-CoA carboxylase1 (ACC1) and phosphorylated ACC1 (Ser79, p-ACC1) in temporalis muscle of naked mole-rats exposed to 4 h hypoxia. (B) Immunoblots of protein expression from A. Data in A are means±s.e.m. from *n*=6 independent biological replicates for each condition. Significant differences from normoxic controls are indicated by asterisks (**P*<0.05, unpaired Student's *t*-test).

phosphorylation and suggest that AMPK mediates a hypoxic downregulation of glycolytic metabolism in this tissue. Conversely, we found no change in ACC1 or p-ACC1. When phosphorylated at Ser79 by AMPK, ACC1 activity is inhibited, which in turn halts fatty acid synthesis (Gusarova et al., 2009). The constant levels of p-ACC1 during hypoxia suggest that this downstream target of AMPK is not modified during hypoxia, and that fatty acid biosynthetic pathways are not altered.

These results differ from previous reports in skeletal muscle of hypoxia-intolerant mice, in which hypoxia activates AMPK, increases GLUT4 expression and increases carbohydrate uptake into cells, whereas a dominant inhibitory mutant of AMPK prevented these changes in hypoxia (Mu et al., 2001). Indeed, AMPK is broadly activated as a result of energy imbalance during hypoxia, with evidence supporting this relationship in brain, liver, skeletal muscle, cardiomyocytes, alveolar and intestinal epithelial cells, and fibroblasts from various hypoxia-intolerant species (Dengler, 2020), along with downstream activation of glucose uptake into cells and altered fatty acid metabolism, among other effects. Indeed, to the best of our knowledge, ours is the first report of AMPK being actively downregulated during hypoxia in any tissue of any species.

AMPK-associated miRNAs are hypoxia responsive in skeletal muscle

A key reason for the divergent response between naked mole-rat skeletal muscle and various tissues in hypoxia-intolerant species may be that ATP is not depleted during severe hypoxia in naked mole-rat skeletal muscle (Pamenter et al., 2019), as is generally the case during periods of oxygen scarcity (or anaerobic exercise). Given the absence of a cellular energy imbalance to alter AMPK activity in hypoxic skeletal muscle, and the atypical decrease in AMPK function in this tissue, we examined a potential novel role for miRNAs in negatively regulating AMPK in hypoxia. We found that the expression of most AMPK-associated miRNAs does not change in naked mole-rat skeletal muscle during hypoxia; however, 10 miRNAs that are associated with key regulatory aspects of AMPK and downstream AMPK signalling were altered in our experiments. Of the three miRNAs that were upregulated in hypoxia, miR-124 is implicated in AMPK phosphorylation, as suppression of this miRNA increases p-AMPK protein levels (Gong et al., 2016; He et al., 2020), while overexpression of miR-124 is linked to a reduction in cell proliferation via G1-phase cell cycle arrest, which is an energy-expensive cellular process that can be

Journal of Experimental Biology (2021) 224, jeb242968. doi:10.1242/jeb.242968

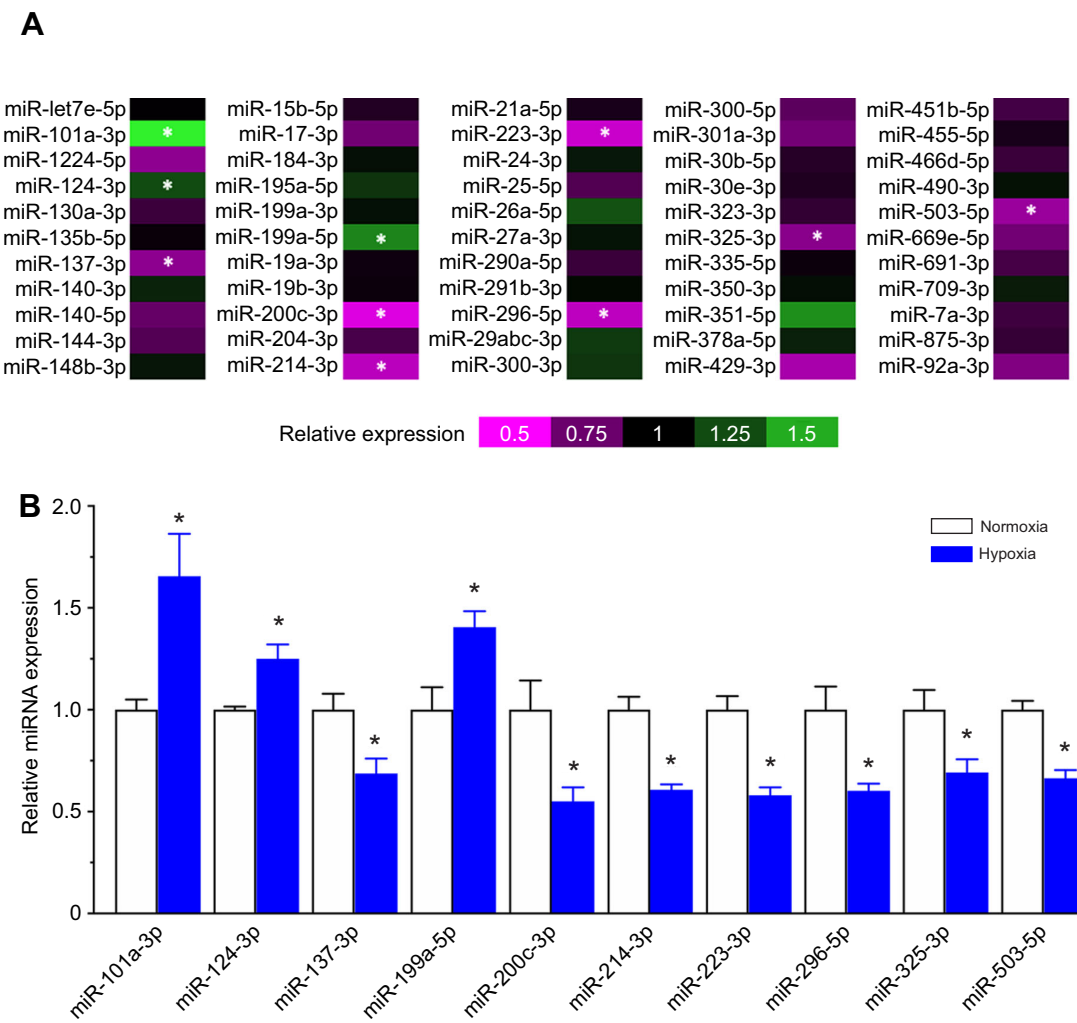

Fig. 4. AMPK-regulating microRNA (miRNA) expression is altered in naked mole-rats after acute hypoxia. (A) Heatmap of the relative expression levels (versus normoxia) from qPCR of 55 AMPK-associated miRNAs in naked mole-rat temporalis muscle tissue following 4 h hypoxia. (B) miRNAs that showed a significant change in expression following hypoxia (P<0.05). Data are means±s.e.m. from n=3–4 independent biological replicates for each condition. Significant differences from normoxic controls are indicated by asterisks (*P<0.05, unpaired Student's t-test). Refer to Table S2 for mean±s.e.m. relative expression values of all 55 miRNAs.

halted during hypoxic energy-conserving states (Lang and Ling, 2012). In addition, miR-124 over-expression also decreases both cell growth and glucose consumption in cancer cells (Zhao et al., 2017), consistent with a downregulation of AMPK. Similarly, upregulated levels of miR-101a and miR-199a are associated with reductions in AMPK signalling (Li et al., 2020), and miR-101a can both directly and indirectly inactivate AMPK (Li et al., 2018; Liu et al., 2016). The seven miRNAs that were downregulated during hypoxia are also implicated in AMPK signalling, primarily downstream of direct regulation of the kinase, and play important roles in alleviating oxidative stress, autophagy and apoptosis during hypoxia, or following anoxia/reoxygenation (da Cruz et al., 2018; Li et al., 2016; Sun et al., 2018; Tran et al., 2017; Zhao et al., 2020; Zhu et al., 2018). Intriguingly, downregulation of miR-223 is also associated with downregulation of GLUT4 protein expression (Lu et al., 2010), concurring with our findings.

A mechanism for tissue-specific energy prioritization in hypoxia?

Importantly, naked mole-rats mobilize glucose from the liver to the blood during severe hypoxia (Pamenter et al., 2019). If muscle is not utilizing this carbohydrate fuel, then where is it going? One promising explanation is that this fuel is being prioritized for use by the brain, which is highly sensitive to energy depletion in hypoxia; by reducing glucose uptake and use by muscle cells, circulating glucose would remain available to more hypoxia-sensitive tissues. In support of this, we have previously reported that brain ATP concentrations fall in severe hypoxia (Pamenter et al., 2019), which is a canonical activator of AMPK. Furthermore, in a previous study we assayed changes in 200+ miRNAs in naked mole-rat brain following acute *in vivo* hypoxia (4 h at 7% O_2) (Hadj-Moussa et al., 2021). These miRNAs include 19 of the 55 AMPK-related transcripts that were assayed in the present study. Of these 19, 6 were significantly downregulated in hypoxic brain and none were upregulated (P<0.10), including miR-124-3p (P=0.084), which is upregulated in muscle, and miR-140-3P (P=0.069), miR-140-5p (P=0.033), miR-19b-3p (P=0.046) and miR-301a-3p (P=0.016), all of which are unchanged in muscle. Notably, the downregulation of each of these 5 miRNAs in the brain correlates with increased AMPK activity (Bhardwaj et al., 2018; Gong et al., 2016; He et al., 2020; Sun et al., 2019; Yeon et al., 2019). In addition, miR-199a-5p and miR-223-3p, which were upregulated and downregulated in

muscle, respectively (see above), are unchanged in brain (Hadj-Moussa et al., 2021). Finally, miR-325-3p is downregulated in both tissues, but the impact of this miRNA on AMPK function is unclear.

Taken together, these data support the hypothesis that AMPK is upregulated in naked mole-rat brain during hypoxia, in direct contrast to the changes observed in skeletal muscle. This relationship hints at a potential mechanism via which miRNAs may mediate tissue-specific metabolic fuel switches in hypoxic naked mole-rats, and support prioritization of limited energetic resources for more vulnerable and essential organs during severe hypoxia. Further experiments in the brain are warranted to explore hypoxia-mediated changes in AMPK phosphorylation and downstream changes in GLUTs and both glycolytic and fatty acid oxidation enzymes.

Interestingly, AMPK may similarly regulate tissue-specific metabolism in other hypoxia-tolerant species, but the scarce information available presents a variable pattern. For example, AMPK is activated in goldfish (*Carassius auratus*) liver during 12 h of severe hypoxia, but is not altered in muscle, brain, heart or gill (Jibb and Richards, 2008). Similarly, in anoxia-tolerant crucian carp (*Carassius carassius*), AMPK phosphorylation is slightly increased in the brain and heart following 10 days of hypoxia but is markedly increased following 10 days of anoxia (Stensløkken et al., 2008). In anoxia-tolerant red-eared slider turtles (*Trachemys scripta elegans*), AMPK is phosphorylated in white muscle and heart, but is unchanged in liver and red muscle following 20 h of anoxia (Rider et al., 2009). While these examples demonstrate tissue-specific increases in AMPK-mediated metabolic function in other hypoxia-tolerant species, our finding of coordinated downregulation of AMPK-mediated energetics in skeletal muscle appears unique and also provides a potential regulatory mechanism.

Conclusions

Aerobic energy production is significantly impaired during periods of low-oxygen stress and anaerobic metabolism is less efficient and leads to the build-up of potentially deleterious end-products, which must be catabolized via energetically expensive processes upon reoxygenation. For animals that live in intermittent hypoxia, metabolic downregulation is a more efficient and common strategy than upregulation of anaerobic pathways (Boutilier, 2001; Buck and Pamenter, 2006; Hochachka et al., 1996). However, across organ systems, oxygen availability and metabolic capacity must often be prioritized for key tissues, particularly the heart and brain, which must remain functional in hypoxia. Conversely, skeletal muscle, which often functions via anaerobic metabolism during intense exercise, is more tolerant of localized hypoxia and thus shutting down metabolism in this tissue offers a means to conserve and redirect energy towards more vital organs in severely hypoxic conditions. Although others have suggested that hypoxic species prioritize the energy demands of the heart and brain over those of the muscle, no previous study has demonstrated an inhibition of AMPK signalling during hypoxia in any tissue. Our results in naked mole-rat skeletal muscle, and comparison with previous analysis in hypoxic naked mole-rat brain, suggest that miRNA may offer such a mechanism and coordinate the AMPK-signalling axis to locally regulate metabolic demand at the tissue level, thereby driving metabolic reorganization to prioritize key organs during periods of severe hypoxia.

Acknowledgements

We would like to thank the University of Ottawa animal care and veterinary services teams for their assistance in animal handling and husbandry.

Competing interests

The authors declare no competing or financial interests.

Author contributions

Conceptualization: M.E.P.; Methodology: H.H.-M., K.B.S., M.E.P.; Software: H.H.-M.; Validation: H.H.-M., M.E.P.; Formal analysis: H.H.-M., S.C.; Investigation: H.H.-M., S.C., H.C., L.E., M.E.P.; Resources: K.B.S., M.E.P.; Data curation: H.H.-M., M.E.P.; Writing - original draft: H.H.-M., M.E.P.; Writing - review & editing: H.H.-M., K.B.S., M.E.P.; Supervision: K.B.S., M.E.P.; Project administration: K.B.S., M.E.P.; Funding acquisition: K.B.S., M.E.P.

Funding

This work was supported by Discovery Grants to K.B.S. [6793] and to M.E.P. [04229] from the Natural Sciences and Engineering Research Council of Canada (NSERC). K.B.S. holds the Canada Research Chair in Molecular Physiology, M.E.P. held the Canada Research Chair in Comparative Neurophysiology and H.H.-M. holds an Ontario Graduate Scholarship.

References

Abbud, W., Habinowski, S., Zhang, J.-Z., Kendrew, J., Elkairi, F. S., Kemp, B. E., Witters, L. A. and Ismail-Beigi, F. (2000). Stimulation of AMP-activated protein kinase (AMPK) is associated with enhancement of Glut1-mediated glucose transport. *Arch. Biochem. Biophys.* **380**, 347-352. doi:10.1006/abbi.2000.1935

Bhardwaj, A., Singh, H., Trinidad, C. M., Albarracin, C. T., Hunt, K. K. and Bedrosian, I. (2018). The isomiR-140-3p-regulated mevalonic acid pathway as a potential target for prevention of triple negative breast cancer. *Breast Cancer Res.* **20**, 150. doi:10.1186/s13058-018-1074-z

Biggar, K. K., Wu, C.-W. and Storey, K. B. (2014). High-throughput amplification of mature microRNAs in uncharacterized animal models using polyadenylated RNA and stem-loop reverse transcription polymerase chain reaction. *Anal. Biochem.* **462**, 32-34. doi:10.1016/j.ab.2014.05.032

Boutilier, R. G. (2001). Mechanisms of cell survival in hypoxia and hypothermia. *J. Exp. Biol.* **204**, 3171-3181. doi:10.1242/jeb.204.18.3171

Buck, L. T. and Pamenter, M. E. (2006). Adaptive responses of vertebrate neurons to anoxia–matching supply to demand. *Respir. Physiol. Neurobiol.* **154**, 226-240. doi:10.1016/j.resp.2006.03.004

Bustin, S. A., Benes, V., Garson, J. A., Hellemans, J., Huggett, J., Kubista, M., Mueller, R., Nolan, T., Pfaffl, M. W., Shipley, G. L. et al. (2009). The MIQE guidelines: minimum information for publication of quantitative real-time PCR experiments. *Clin. Chem.* **55**, 611-622. doi:10.1373/clinchem.2008.112797

Chung, D., Dzal, Y. A., Seow, A., Milsom, W. K. and Pamenter, M. E. (2016). Naked mole rats exhibit metabolic but not ventilatory plasticity following chronic sustained hypoxia. *Proc. Biol. Sci.* **283**. doi:10.1098/rspb.2016.0216

da Cruz, R. S., Carney, E. J., Clarke, J., Cao, H., Cruz, M. I., Benitez, C., Jin, L., Fu, Y., Cheng, Z., Wang, Y. et al. (2018). Paternal malnutrition programs breast cancer risk and tumor metabolism in offspring. *Breast Cancer Res.* **20**, 99. doi:10.1186/s13058-018-1034-7

Dengler, F. (2020). Activation of AMPK under hypoxia: many roads leading to Rome. *Int. J. Mol. Sci.* **21**, 2428. doi:10.3390/ijms21072428

Dzal, Y. A., Seow, A., Borecky, L. G., Chung, D., Gill, S. K. G., Milsom, W. K. and Pamenter, M. E. (2019). Glutamatergic receptors modulate normoxic but not hypoxic ventilation and metabolism in naked mole rats. *Front. Physiol.* **10**, 106. doi:10.3389/fphys.2019.00106

Gong, X., Wang, H., Ye, Y., Shu, Y., Deng, Y., He, X., Lu, G. and Zhang, S. (2016). miR-124 regulates cell apoptosis and autophagy in dopaminergic neurons and protects them by regulating AMPK/mTOR pathway in Parkinson's disease. *Am. J. Transl. Res.* **8**, 2127-2137.

Gusarova, G. A., Dada, L. A., Kelly, A. M., Brodie, C., Witters, L. A., Chandel, N. S. and Sznajder, J. I. (2009). Alpha1-AMP-activated protein kinase regulates hypoxia-induced Na,K-ATPase endocytosis via direct phosphorylation of protein kinase Cζ. *Mol. Cell. Biol.* **29**, 3455-3464. doi:10.1128/MCB.00054-09

Ha, J., Guan, K.-L. and Kim, J. (2015). AMPK and autophagy in glucose/glycogen metabolism. *Mol. Aspects Med.* **46**, 46-62. doi:10.1016/j.mam.2015.08.002

Hadj-Moussa, H. and Storey, K. B. (2018). Micromanaging freeze tolerance: the biogenesis and regulation of neuroprotective microRNAs in frozen brains. *Cell. Mol. Life Sci.* **75**, 3635-3647. doi:10.1007/s00018-018-2821-0

Hadj-Moussa, H. and Storey, K. B. (2020). The OxymiR response to oxygen limitation: a comparative microRNA perspective. *J. Exp. Biol.* **223**, jeb204594. doi:10.1242/jeb.204594

Hadj-Moussa, H., Zhang, J., Pifferi, F., Perret, M. and Storey, K. B. (2020). Profiling torpor-responsive microRNAs in muscles of the hibernating primate Microcebus murinus. *Biochim. Biophys. Acta Gene Regul. Mech.* **1863**, 194473. doi:10.1016/j.bbagrm.2019.194473

Hadj-Moussa, H., Pamenter, M. E. and Storey, K. B. (2021). Hypoxic naked mole-rat brains use microRNA to coordinate hypometabolic fuels and neuroprotective defenses. *J. Cell. Physiol.* **236**, 5080-5097. doi:10.1002/jcp.30216

Hardie, D. G. (2007). AMP-activated/SNF1 protein kinases: conserved guardians of cellular energy. *Nat. Rev. Mol. Cell Biol.* **8**, 774-785. doi:10.1038/nrm2249

Hardie, D. G., Ross, F. A. and Hawley, S. A. (2012). AMPK: a nutrient and energy sensor that maintains energy homeostasis. *Nat. Rev. Mol. Cell Biol.* **13**, 251-262. doi:10.1038/nrm3311

He, Y., Yang, Y., Liao, Y., Xu, J., Liu, L., Li, C. and Xiong, X. (2020). miR-140-3p inhibits cutaneous melanoma progression by disrupting AKT/p70S6K and JNK pathways through ABHD2. *Mol. Ther. Oncolytics* **17**, 83-93. doi:10.1016/j.omto.2020.03.009

Hochachka, P. W., Buck, L. T., Doll, C. J. and Land, S. C. (1996). Unifying theory of hypoxia tolerance: molecular/metabolic defense and rescue mechanisms for surviving oxygen lack. *Proc. Natl. Acad. Sci. USA* **93**, 9493-9498. doi:10.1073/pnas.93.18.9493

Holmes, M. M., Goldman, B. D., Goldman, S. L., Seney, M. L. and Forger, N. G. (2009). Neuroendocrinology and sexual differentiation in eusocial mammals. *Front. Neuroendocrinol.* **30**, 519-533. doi:10.1016/j.yfrne.2009.04.010

Holtze, S., Braude, S., Lemma, A., Koch, R., Morhart, M., Szafranski, K., Platzer, M., Alemayehu, A., Goeritz, F. and Hildebrandt, T. B. (2018). The microenvironment of naked mole-rat burrows in East Africa. *Afr. J. Ecol.* **56**, 279-289. doi:10.1111/aje.12448

Houlahan, C. R., Kirby, A. M., Dzal, Y. A., Fairman, G. D. and Pamenter, M. E. (2018). Divergent behavioural responses to acute hypoxia between individuals and groups of naked mole rats. *Comp. Biochem. Physiol. B Biochem. Mol. Biol.* **224**, 38-44. doi:10.1016/j.cbpb.2018.01.004

Ilacqua, A. N., Kirby, A. M. and Pamenter, M. E. (2017). Behavioural responses of naked mole rats to acute hypoxia and anoxia. *Biol. Lett.* **13**. doi:10.1098/rsbl.2017.0545

Jibb, L. A. and Richards, J. G. (2008). AMP-activated protein kinase activity during metabolic rate depression in the hypoxic goldfish, Carassius auratus. *J. Exp. Biol.* **211**, 3111-3122. doi:10.1242/jeb.019117

Kahn, B. B., Alquier, T., Carling, D. and Hardie, D. G. (2005). AMP-activated protein kinase: ancient energy gauge provides clues to modern understanding of metabolism. *Cell Metab.* **1**, 15-25. doi:10.1016/j.cmet.2004.12.003

Kirby, A. M., Fairman, G. D. and Pamenter, M. E. (2018). Atypical behavioural, metabolic and thermoregulatory responses to hypoxia in the naked mole rat (Heterocephalus glaber). *J. Zool.* **305**, 106-115. doi:10.1111/jzo.12542

Lang, Q. and Ling, C. (2012). MiR-124 suppresses cell proliferation in hepatocellular carcinoma by targeting PIK3CA. *Biochem. Biophys. Res. Commun.* **426**, 247-252. doi:10.1016/j.bbrc.2012.08.075

Li, J., Li, J., Wei, T. and Li, J. (2016). Down-regulation of microRNA-137 improves high glucose-induced oxidative stress injury in human umbilical vein endothelial cells by up-regulation of AMPKalpha1. *Cell. Physiol. Biochem.* **39**, 847-859. doi:10.1159/000447795

Li, Y., Wang, S., Gao, X., Zhao, Y., Li, Y., Yang, B., Zhang, N. and Ma, L. (2018). Octreotide alleviates autophagy by up-regulation of microRNA-101 in intestinal epithelial cell line Caco-2. *Cell. Physiol. Biochem.* **49**, 1352-1363. doi:10.1159/000493413

Li, Y., Luan, Y., Li, J., Song, H., Li, Y., Qi, H., Sun, B., Zhang, P., Wu, X., Liu, X. et al. (2020). Exosomal miR-199a-5p promotes hepatic lipid accumulation by modulating MST1 expression and fatty acid metabolism. *Hepatol Int* **14**, 1057-1074. doi:10.1007/s12072-020-10096-0

Lighton, J. (2008). *Measuring Metabolic Rates: A Manual for Scientists*. Oxford: Oxford University Press.

Liu, P., Ye, F., Xie, X., Li, X., Tang, H., Li, S., Huang, X., Song, C., Wei, W. and Xie, X. (2016). mir-101-3p is a key regulator of tumor metabolism in triple negative breast cancer targeting AMPK. *Oncotarget* **7**, 35188-35198. doi:10.18632/oncotarget.9072

Lu, H., Buchan, R. J. and Cook, S. A. (2010). MicroRNA-223 regulates Glut4 expression and cardiomyocyte glucose metabolism. *Cardiovasc. Res.* **86**, 410-420. doi:10.1093/cvr/cvq010

Mu, J., Brozinick, J. T., , Jr, Valladares, O., Bucan, M. and Birnbaum, M. J. (2001). A role for AMP-activated protein kinase in contraction- and hypoxia-regulated glucose transport in skeletal muscle. *Mol. Cell* **7**, 1085-1094. doi:10.1016/S1097-2765(01)00251-9

O'Brien, J., Hayder, H., Zayed, Y. and Peng, C. (2018). Overview of MicroRNA Biogenesis, Mechanisms of Actions, and Circulation. *Front. Endocrinol. (Lausanne)* **9**, 402. doi:10.3389/fendo.2018.00402

Pamenter, M. E., Dzal, Y. A. and Milsom, W. K. (2015). Adenosine receptors mediate the hypoxic ventilatory response but not the hypoxic metabolic response in the naked mole rat during acute hypoxia. *Proc. Biol. Sci.* **282**, 20141722. doi:10.1098/rspb.2014.1722

Pamenter, M. E., Lau, G. Y., Richards, J. G. and Milsom, W. K. (2018). Naked mole rat brain mitochondria electron transport system flux and H(+) leak are reduced during acute hypoxia. *J. Exp. Biol.* **221**, jeb171397. doi:10.1242/jeb.171397

Pamenter, M. E., Dzal, Y. A., Thompson, W. A. and Milsom, W. K. (2019). Do naked mole rats accumulate a metabolic acidosis or an oxygen debt in severe hypoxia? *J. Exp. Biol.* **222**, jeb191197. doi:10.1242/jeb.191197

Park, T. J., Reznick, J., Peterson, B. L., Blass, G., Omerbasic, D., Bennett, N. C., Kuich, P. H. J. L., Zasada, C., Browe, B. M., Hamann, W. et al. (2017). Fructose-driven glycolysis supports anoxia resistance in the naked mole-rat. *Science* **356**, 305-308. doi:10.1126/science.aab3896

Peltier, H. J. and Latham, G. J. (2008). Normalization of microRNA expression levels in quantitative RT-PCR assays: identification of suitable reference RNA targets in normal and cancerous human solid tissues. *RNA* **14**, 844-852. doi:10.1261/rna.939908

Rider, M. H. (2016). Role of AMP-activated protein kinase in metabolic depression in animals. *J. Comp. Physiol. B* **186**, 1-16. doi:10.1007/s00360-015-0920-x

Rider, M. H., Hussain, N., Dilworth, S. M. and Storey, K. B. (2009). Phosphorylation of translation factors in response to anoxia in turtles, Trachemys scripta elegans: role of the AMP-activated protein kinase and target of rapamycin signalling pathways. *Mol. Cell. Biochem.* **332**, 207-213. doi:10.1007/s11010-009-0193-3

Ross, F. A., MacKintosh, C. and Hardie, D. G. (2016). AMP-activated protein kinase: a cellular energy sensor that comes in 12 flavours. *FEBS J.* **283**, 2987-3001. doi:10.1111/febs.13698

Schmittgen, T. D. and Livak, K. J. (2008). Analyzing real-time PCR data by the comparative C(T) method. *Nat. Protoc.* **3**, 1101-1108. doi:10.1038/nprot.2008.73

Stensløkken, K.-O., Ellefsen, S., Stecyk, J. A. W., Dahl, M. B., Nilsson, G. E. and Vaage, J. (2008). Differential regulation of AMP-activated kinase and AKT kinase in response to oxygen availability in crucian carp (Carassius carassius). *Am. J. Physiol. Regul. Integr. Comp. Physiol.* **295**, R1803-R1814. doi:10.1152/ajpregu.90590.2008

Sun, T., Li, M.-Y., Li, P.-F. and Cao, J.-M. (2018). MicroRNAs in cardiac autophagy: small molecules and big role. *Cells* **7**, 104. doi:10.3390/cells7080104

Sun, Y., Song, Y., Liu, C. and Geng, J. (2019). LncRNA NEAT1-MicroRNA-140 axis exacerbates nonalcoholic fatty liver through interrupting AMPK/SREBP-1 signaling. *Biochem. Biophys. Res. Commun.* **516**, 584-590. doi:10.1016/j.bbrc.2019.06.104

Suter, M., Riek, U., Tuerk, R., Schlattner, U., Wallimann, T. and Neumann, D. (2006). Dissecting the role of 5′-AMP for allosteric stimulation, activation, and deactivation of AMP-activated protein kinase. *J. Biol. Chem.* **281**, 32207-32216. doi:10.1074/jbc.M606357200

Tran, M., Lee, S.-M., Shin, D.-J. and Wang, L. (2017). Loss of miR-141/200c ameliorates hepatic steatosis and inflammation by reprogramming multiple signaling pathways in NASH. *JCI Insight* **2**. doi:10.1172/jci.insight.96094

Vandewint, A. L., Zhu-Pawlowsky, A. J., Kirby, A., Tattersall, G. J. and Pamenter, M. E. (2019). Evaporative cooling and vasodilation mediate thermoregulation in naked mole-rats during normoxia but not hypoxia. *J. Therm. Biol.* **84**, 228-235. doi:10.1016/j.jtherbio.2019.07.011

Winder, W. W., Hardie, D. G., Mustard, K. J., Greenwood, L. J., Paxton, B. E., Park, S. H., Rubink, D. S. and Taylor, E. B. (2003). Long-term regulation of AMP-activated protein kinase and acetyl-CoA carboxylase in skeletal muscle. *Biochem. Soc. Trans.* **31**, 182-185. doi:10.1042/bst0310182

Yeon, M., Lee, S., Lee, J.-E., Jung, H. S., Kim, Y. and Jeoung, D. (2019). CAGE-miR-140-5p-Wnt1 axis regulates autophagic flux, tumorigenic potential of mouse colon cancer cells and cellular interactions mediated by exosomes. *Front. Oncol.* **9**, 1240. doi:10.3389/fonc.2019.01240

Zhang, J. and Storey, K. B. (2016). RBioplot: an easy-to-use R pipeline for automated statistical analysis and data visualization in molecular biology and biochemistry. *PeerJ* **4**, e2436. doi:10.7717/peerj.2436

Zhang, J.-Z., Behrooz, A. and Ismail-Beigi, F. (1999). Regulation of glucose transport by hypoxia. *Am. J. Kidney Dis.* **34**, 189-202. doi:10.1016/S0272-6386(99)70131-9

Zhao, X., Lu, C., Chu, W., Zhang, B., Zhen, Q., Wang, R., Zhang, Y., Li, Z., Lv, B., Li, H. et al. (2017). MicroRNA-124 suppresses proliferation and glycolysis in non-small cell lung cancer cells by targeting AKT-GLUT1/HKII. *Tumour Biol.* **39**, 1010428317706215. doi:10.1177/1010428317706215

Zhao, T., Qiu, Z. and Gao, Y. (2020). MiR-137-3p exacerbates the ischemia-reperfusion injured cardiomyocyte apoptosis by targeting KLF15. *Naunyn Schmiedebergs Arch. Pharmacol.* **393**, 1013-1024. doi:10.1007/s00210-019-01728-w

Zhu, W., Lei, J., Bai, X., Wang, R., Ye, Y. and Bao, J. (2018). MicroRNA-503 regulates hypoxia-induced cardiomyocytes apoptosis through PI3K/Akt pathway by targeting IGF-1R. *Biochem. Biophys. Res. Commun.* **506**, 1026-1031. doi:10.1016/j.bbrc.2018.10.160